NJC

ROYAL SOCIETY OF CHEMISTRY

PAPER

View Article Online
View Journal | View Issue

Check for updates

Cite this: *New J. Chem.*, 2021, 45, 16883

Application of reduced graphene oxide-based actuators for real-time chemical sensing of liquid and vapour phase contaminants†

Arindom Bikash Neog,[a] Raj Kumar Gogoi,[a] Priyamjeet Deka,[b] Tukhar Jyoti Konch,[a] Barsha Rani Bora[a] and Kalyan Raidongia *[ac]

Received 18th June 2021,
Accepted 6th August 2021

DOI: 10.1039/d1nj02988f

rsc.li/njc

Real-time detection of contaminants dissolved in a liquid medium is critical for various technological and industrial operations. Here, we have demonstrated the possibility of employing reconstructed layered material-based responsive membranes for the *in situ* detection of chemical contaminants in the liquid phase. A bilayer membrane prepared by sequential vacuum filtration of reduced graphene oxide (r-GO) and agar (r-GO/agar) displayed remarkable responsiveness towards the presence of solvent vapours in their surrounding atmosphere. The shape-morphing property of the r-GO/agar membrane is attributed to unequal changes in the mechanical properties of the individual components. Rectangular strips of the bilayer membrane also displayed shape-transforming properties inside the liquid medium. Depending upon the chemical nature of the molecules, inside the liquid medium, the strips of r-GO/agar membrane bend at a definite speed to adopt a coil-like shape. The original shape of the strip is easily recovered after dipping in water or drying in air. The bending angle and the response time of the r-GO/agar strips were found to be sensitive towards trace amounts of impurities present in the solvent system, which can be exploited for the detection of contaminants in the liquid phase, like trace amounts of water molecules dissolved in acetone or different alcohol molecules dissolved in toluene.

Introduction

The development of novel systems capable of detecting a trace amount of liquid inside another liquid medium is considered to be imperative for technological/industrial operations.[1,2] For example, the detection of a trace amount of an aqueous impurity in organic solvents is crucial for maintaining the safety of chemical laboratories as well as in the production of pharmaceuticals and other essential chemical compounds.[3,4] Similarly, the detection of organic contaminants in an aqueous medium is crucial for monitoring environmental water bodies, drinking water technologies, and food-related industries.[5–8] Accurate information about water content in oil also provides valuable inputs about the dynamic behaviour of different emulsion-based systems.[1,9,10] Likewise, aqueous contaminants critically affect the performance of lubricants, and above the accepted levels of water content, lubricants lead to abrasive wear and corrosion of machinery.[2]

Due to its practical importance, novel techniques have been investigated for easy, quick, and real-time detection of liquid molecules inside the matrix of another liquid. The notable examples include photoluminescence (PL)-based sensing, NMR spectroscopy-based techniques, and titration-based methods. The PL-based methods involve changes in the luminescence properties of fluorophores upon contact with water molecules, which is detected by using a fluorimeter instrument. Typical fluorophores used for this purpose are based on quantum dots, fluorescent organic molecules, metal–organic hybrid materials, metal–organic frameworks, polymers, and ceramics.[8,11–16] Similarly, in ^{19}F NMR spectroscopy-based sensing, anhydrous fluoride reagents are employed for the detection of a trace amount of water molecules dissolved in organic solvents.[17] All these processes involve highly complicated and complex synthesis procedures as well as expensive instrumentation.[18] Moreover, the organic water probes used in these methods are hardly recoverable and hence not suitable for long-term use.[4] Here, we propose an alternative method for the real-time detection of a trace amount of chemicals mixed in another liquid medium just by monitoring the shape of a smart material.

Due to their wide range of application possibilities in diverse areas such as sensing,[19] robotics,[20] drug delivery,[21] artificial muscles,[22] and space technology,[23] smart materials have been fabricated from a variety of materials such as polymers,[24]

[a] *Department of Chemistry, Indian Institute of Technology Guwahati, Guwahati-781039, Assam, India. E-mail: k.raidongia@iitg.ac.in*
[b] *School of Energy Science and Engineering, Indian Institute of Technology Guwahati, Guwahati-781039, Assam, India*
[c] *Centre for Nanotechnology, Indian Institute of Technology Guwahati, Guwahati-781039, Assam, India*

† Electronic supplementary information (ESI) available. See DOI: 10.1039/d1nj02988f

alloys,[25] ceramics,[26] and nanomaterials.[27] Very recently, smart bilayer membranes were also prepared by assembling exfoliated layers of two-dimensional materials.[28,29] Layered materials such as graphite, V_2O_5, MOS_2, and clays are composed of 2D sheets stacked together through weak forces such as van der Waals attractions or hydrogen bonding. These 2D sheets can be exfoliated into individual nanosheets and re-assembled into macroscopic membranes known as reconstructed layered materials. The smart materials prepared by reconstructing layered materials exhibit several advantages, such as easy fabrication techniques, both pre- and post-assembly modification possibility, facile scalability, high-sensitivity and robustness.[19,28–31] The notable examples of bilayer membrane-based smart materials include strips of GO-r-GO-,[32,33] GO/CNT-,[34] vermiculite/GO-,[29] vermiculite/montmorillonite-28 and GO/PPy(polypyrrole)[35]-based bilayer membranes, and all of these membranes demonstrated highly reversible shape-morphing characteristics towards multiple stimuli such as the vapours of organic solvents, humidity, and temperature and light.[28,29] Most of the smart materials prepared by reconstructing layered materials demonstrate responsiveness only in an air atmosphere, and not inside a liquid medium. Exceptional examples include asymmetrically modified graphene film-based actuators and bilayer membranes of vermiculite/graphene oxide. Strips of surface-modified graphene films demonstrate a reversible swing motion upon cyclic voltammogramic (CV) scanning inside a 1 M $NaClO_4$ electrolyte.[36] Analogous actuation properties were also reported with strips cut out from a PPy/graphene bilayer film.[37] The bilayer membranes of vermiculite/graphene oxide also exhibited a reversible bending behaviour inside a solvent medium of contrasting polarity.[29] Similarly, a few polymer-based materials have also shown responsiveness inside a liquid medium; however, these materials are yet to be investigated for the detection of contaminants or impurities in a liquid medium.[38–41] To the best of our knowledge, reconstructed bilayer membrane-based actuators have not been employed so far for detecting trace amounts of liquid molecules dispersed in another liquid medium. Here, we report the fabrication of a responsive bilayer membrane through sequential vacuum filtration of reduced graphene oxide (r-GO) and agar dispersions. U-shaped strips of similar r-GO/agar bilayer membrane were also exploited for inducing chemical reactions in microdroplets by using electrical potential and infrared light as the remote handles.[42] Multiple r-GO- and GO-based composites were also investigated for different kinds of sensing applications, such as the photoelectrochemical sensing of prostate-specific antigens and the screening of H_2S.[43–47] However, all these applications require sophisticated instrumentation and are only applicable for very specific systems. The bilayer strips of r-GO/agar have demonstrated excellent responsiveness inside a liquid medium and have shown the capability of detecting trace amounts of liquid contaminants inside another liquid. The r-GO/agar membrane has the potential to be applied in areas such as sensing under a liquid medium and for the detection of chemical vapours under ambient atmospheric conditions.

Results and discussion

Multi-responsive bilayer membranes of reduced graphene oxide and agar (r-GO/agar) were prepared by vacuum filtering a dispersion of agar (in DMF) through a reconstructed r-GO membrane.[42] The r-GO fraction of the membrane was prepared through the reduction of graphene oxide (GO) by heating its dispersion (0.5 mg mL^{-1} in DMF) at 153 °C for 2 hours. A digital photo of the starting GO dispersion (inset of Fig. 1a) and an AFM image of the flakes are shown in Fig. 1a. The reduction process did not seem to affect the dispersibility and average dimensions of the flakes, and a representative AFM image is shown in Fig. 1b. The vacuum filtration of the r-GO dispersion in DMF (inset of Fig. 1b) through a hydrophilic PTFE membrane yielded a free-standing r-GO membrane. A homogeneous dispersion of agar was prepared by probe sonicating (1 s on and 1 s off pulses) the mixture (1 mg mL^{-1} in DMF) for 30 minutes.

Thus, the prepared bilayer membrane of r-GO/agar could be easily peeled off from the polytetrafluoroethylene (PTFE) membrane by heating in a hot air oven (70 °C for 2 hours).

Digital images of the r-GO/agar bilayer membrane along with individual free-standing membranes of r-GO and agar are shown in Fig. 1c–e, respectively. Further characterisation of the reconstructed membranes can be found in Fig. S1 (ESI†). While the r-GO side of the r-GO/agar bilayer membrane appears to be greyish-black, the agar-side looks shiny-black in colour. The lamellar r-GO fraction can be easily distinguished from the smoother agar side in the cross-sectional field emission scanning electron microscope (FESEM) image shown in Fig. 1f. The FESEM images of the surface of the agar and r-GO sides of the bilayer membrane are shown in Fig. S3b and d (ESI†), respectively. The surface of the agar side is characterized by a smooth morphology, while that of the r-GO side can be recognized by the wave-like morphology.

The shape of the r-GO/agar membrane was found to be responsive towards the presence of the solvent vapour in its surrounding atmosphere. In order to illustrate the responsiveness of the r-GO/agar membrane, a rectangular strip (dimensions $25 \times 4 \times 0.023$ mm^3) cut from the bilayer membrane was fixed to a rod and exposed to vapours generated from 10 mL of the respective solvents placed in a 250 mL beaker (at 23 °C). A fixed distance of 3 cm was maintained between the strip and the solvent throughout the experiments. Fig. S4 (ESI†) shows the experimental set-up used for studying the solvent vapour-induced responsiveness. Upon exposure to ethyl acetate vapours, the strip immediately recognized the changes in the surroundings and responded by bending towards the agar side. Once the strip was taken away from the vapours, it regained its original shape within 40 seconds of exposure to the open-air atmosphere. To quantify the degree of bending, an imaginary straight line was drawn along the axis of the rod, where the strip was fixed. A schematic illustration of the process is shown in Fig. S5 (ESI†). When the r-GO/agar strip was aligned with that imaginary axis, the bending angle was considered to be zero degree. When it moved towards left, the angle was counted in positive values. When the tip of the strip moved towards right, the

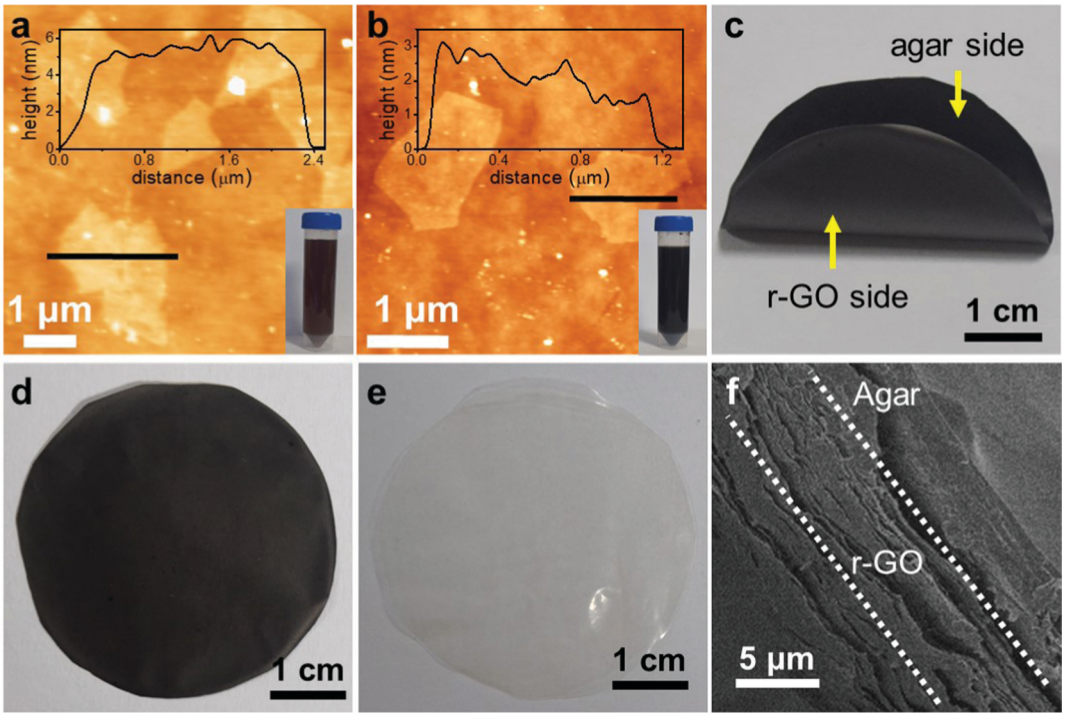

Fig. 1 AFM images (along with the corresponding height profile of the nanosheets and respective dispersions in DMF in the insets) of (a) GO and (b) r-GO nanosheets. Digital photos of the (c) r-GO/agar bilayer, (d) individual r-GO membrane fabricated by the vacuum-assisted filtration method and (e) agar membrane. (f) Cross-sectional FESEM image of the r-GO/agar bilayer membrane.

angle was counted in negative values. The greater the extent of bending, the higher the value of the bending angle. Generally, the r-GO/agar strip bends towards the agar side, which is in the direction of a positive angle. Upon exposure to vapours, it moved towards the agar side, which increases the bending angle in positive values. The changes in the bending angle in the presence of ethyl acetate vapours as a function of time are shown in Fig. S6a (ESI†), and from the slope of this curve, the bending speed of the strip was calculated to be $55^{\circ}\ s^{-1}$. Upon the removal of the ethyl acetate vapours, the strip regained its original configuration with a recovery speed of $77^{\circ}\ s^{-1}$. Fig. 2a and ESI† Video V1 show the bending and recovery movements of the strip induced by the ethyl acetate environment. This solvent-induced responsiveness study was also carried out in the presence of 2-propanol, acetone, tetrahydrofuran (THF), ethanol, chloroform, dichloromethane (DCM) and methanol vapours. The strip responded to the vapours of all the solvents by bending towards the agar side with specific bending speeds. Snapshots of the bending and recovery movements of the strip in the presence of 2-propanol, acetone, THF, ethanol, chloroform, DCM and methanol vapours are shown in Fig. S7a–e and S8a and b (ESI†), respectively. The bending and the recovery speeds of the bilayer strips in the presence of different solvent vapours are compared in Fig. 2b and c, respectively. For each solvent vapour, the bending experiment was repeated for 50 cycles, and the variations in the bending speed between the 1st, 25th and 50th cycles are denoted as the error bars in Fig. 2b.

The shape-morphing properties of these bilayer systems are attributed to an unequal alteration in the mechanical properties of individual components. In order to study the variation in the mechanical properties of the individual components of the bilayer membrane, the bending stiffness values were calculated by using the Lorentzen & Wettre two-point method[28,29] under different environmental conditions. At first, the bending stiffness values of individual membranes were measured under air atmosphere, which was followed by repetition of the measurement after being exposed to a particular solvent vapour. A schematic illustration of the bending stiffness measurement process is shown in Fig. 3a. The changes in the bending stiffness values due to the presence of acetone were calculated and plotted in Fig. 3b and c. The bar diagrams reveal that the r-GO strip displayed a greater decrease (14.4%) in the stiffness values upon exposure to acetone in comparison with that of the agar strip (6.9%). This uneven change in the stiffness values of the two components of the bilayer membrane upon exposure to solvent vapours is attributed to the bending performance. The uneven change in the bending stiffness values in the presence of solvent vapours is attributed to different intercalating natures of the solvent molecules. In order to understand the cause of uneven change in the mechanical properties, the rate of permeation of the solvent vapours through the individual membranes was measured by using a gravimetric method. Typically, two glass vials were filled-up with acetone and sealed with r-GO and agar membranes by using freshly prepared polydimethylsiloxane (PDMS) elastomer as the glue. Both the vials were kept in a closed chamber and were maintained at a constant humidity of 20%. The weights of the vials

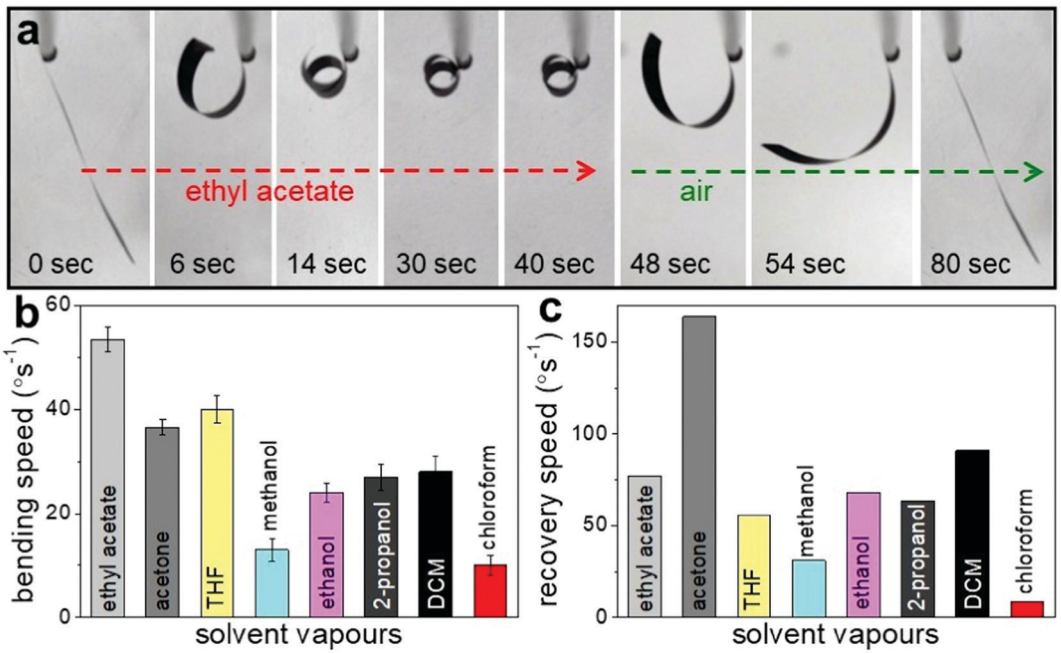

Fig. 2 Vapour-induced shape-morphing characteristics of r-GO/agar bilayer strips: (a) snapshots showing the bending and recovery movements of the bilayer strip upon exposure to ethyl acetate vapours. (b) Bar diagrams representing the bending speeds of the bilayer strip upon exposure to different solvent vapours and (c) the corresponding recovery speeds after the removal of the solvent vapours.

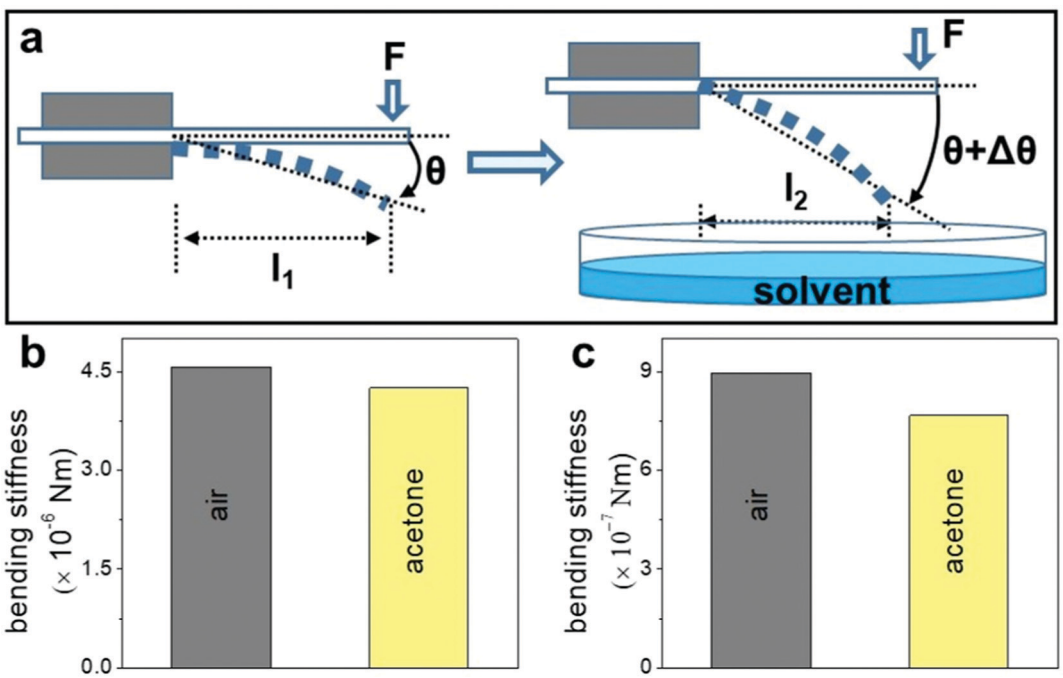

Fig. 3 Bending stiffness of r-GO and agar membranes: (a) a schematic illustration of the bending stiffness measurements in the presence and absence of solvent vapours using the Lorentzen & Wettre two-point method. Bar diagrams demonstrating the bending stiffness of (b) agar and (c) r-GO strips in the absence and presence of acetone vapours.

were taken at regular intervals of time to determine the rate of evaporation of acetone vapours through the individual membranes. As can be observed in Fig. S10 (ESI†), the decrease in weight was found to be higher in the case of the vial covered with the r-GO membrane as compared with the agar membrane, suggesting that acetone can penetrate into the r-GO membrane and alter its properties to an extent greater than that of the agar membrane.

The strips of r-GO/agar bilayer membrane also displayed a remarkable shape-transforming property inside the liquid medium. The responsiveness of the bilayer strip (dimensions 25 × 4 × 0.023 mm^3) was studied by dipping it directly inside the liquid medium. As shown in Fig. 4a and ESI† Video V2, as soon as the r-GO/agar strip was dipped into acetone, it bent towards the agar side forming a loop within ∼ 30 seconds. The strip stayed in that loop shape, as long as it was submerged in liquid acetone. The bending speed of the strip inside liquid acetone was calculated to be 55° s^{-1}. When the r-GO/agar strip was pulled out of the acetone medium and dipped in water, it recovered the original shape within 10 seconds, with a recovery speed of 81° s^{-1}. The snapshots of the bending movement of the bilayer strip inside the acetone–water system are shown in Fig. 4a. Similarly, the solvent-induced responsiveness of the bilayer membrane inside the liquid medium was also investigated with methanol–water, ethanol–water and 2-propanol–water systems, and the snapshots of the bending movements are shown in Fig. S11a–c (ESI†), respectively. Similar to acetone, the strip bent towards the agar side after immerging in liquid methanol, ethanol and 2-propanol, and recovered its original configuration after dipping in water. The bending and recovery speeds of the r-GO/agar strip, after immerging and removing from the liquid medium were found to be specific to the chemical nature of the solvent molecules. For example, in the case of methanol, ethanol and 2-propanol, the bending speeds were calculated to be 50° s^{-1}, 8.5° s^{-1} and 2.7° s^{-1}, respectively. Similarly, the recovery speeds were calculated to be 120.5° s^{-1}, 16° s^{-1} and 12.5° s^{-1}, for methanol, ethanol and 2-propanol media, respectively. The specific bending and recovery speed of the strip with different solvent molecules could lead to a new kind of electronics-free inexpensive sensor of solvent molecules. A comparison of the bending and recovery speeds of the bilayer strip inside different solvent systems is shown in the bar diagrams of Fig. 4b and c, respectively. The bending and recovery experiments inside liquid systems were repeated with a single bilayer strip for 20 cycles and variations in the bending speed between the 1st, 10th and 20th cycles are presented as error bars in Fig. 4b.

In order to understand the mechanism of bending inside the liquid medium, the effects of solvent molecules in the microstructure of the membranes were studied by X-ray diffraction (XRD). As can be observed from the XRD patterns of Fig. S12 (ESI†), the air-dried r-GO strip displayed a broad peak at a 2θ value of ∼ 24°, corresponding to an interlayer space of 3.7 Å (002 reflection). The XRD examination of the r-GO strip was repeated after dipping the same in acetone for 15 minutes. The position of the (002) reflection was found to shift from a 2θ value of 24° to 20° (d = 3.7 Å to 4.4 Å). This increase (0.7 Å) in the interlayer spacing indicates intercalation of acetone molecules into the interlayer galleries of the r-GO membrane. After taking out from acetone, the r-GO strip was again dipped in water for 15 minutes and the microstructures were re-examined by recording the XRD pattern. As can be observed from Fig. S12 (ESI†), the position of the (002) reflection of the r-GO strip shifted back to its original position. Similarly, XRD patterns were also recorded for the agar part of the bilayer strip. The characteristic reflection of the agar at 2θ = 13.1° did not show

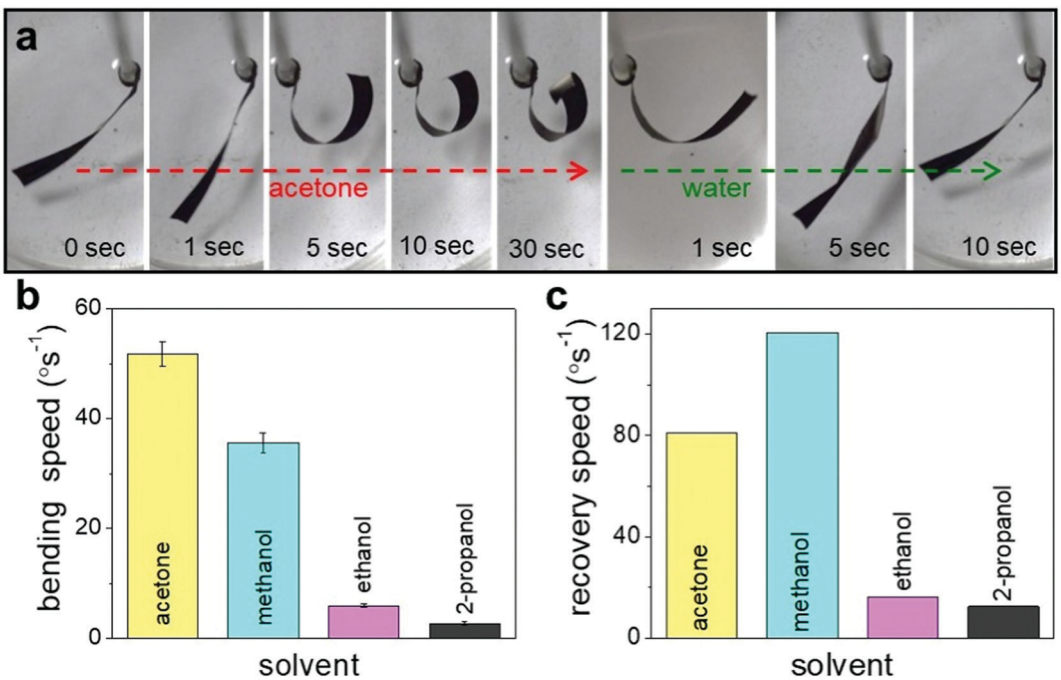

Fig. 4 Solvent-induced shape transformation of r-GO/agar bilayer strips: (a) snapshots showing bending movements in acetone and recovering movements in water of the r-GO/agar bilayer strip. (b) Bar diagrams representing the bending speeds of the bilayer strip inside different solvents and (c) the corresponding recovery speeds when in water.

any definite shift due to subsequent dipping in acetone and water. As can be observed from the XRD patterns, inside the liquid medium, the solvent molecules intercalate into the interlayer spaces of the r-GO strip and alter its *d*-spacing, which would have a definite impact on its mechanical properties. This unequal change in the microstructure of both sides of the bilayer membrane is attributed to the asymmetric bending strain along the membrane, which in turn leads to shape-changing characteristics of the bilayer membrane.

The mechanical properties of the bilayer actuators were studied by recording stress–strain curves before and after periodic soaking and drying of the strips in liquid acetone. The stress–strain curves shown in Fig. S13 (ESI†) confirm that the tensile strength (66 MPa) and Young's modulus (358 MPa) of the pristine bilayer strip did not display significant degradation even after 5 (tensile strength 52 MPa and Young's modulus 352 MPa) and 10 (tensile strength 48 MPa and Young's modulus 347 MPa) dips in acetone. In order to further confirm the strength of the bilayer membrane under liquid medium, its strips were made to lift weights heavier than their own weight. As can be observed from Fig. S14 (ESI†), a strip weighing 2 mg (dimensions $20 \times 3 \times 0.023$ mm^3) could lift 3 mg of weight up to 1.9 cm. Likewise, a strip could lift 5 times it weight up to 1.6 cm. The chemical robustness of the bilayer membrane was also studied after exposing the strips to harsh chemical environments. As can be observed form from Fig. S15 (ESI†), the strips exposed to vapours of concentrated HCl and NH_3 for 6 hours from a distance of 5 cm retained their responsiveness.

The unique bending behaviour of the bilayer membrane can also be utilized to detect trace amounts of liquid contaminants present in a given solvent system. As a proof of concept, the detection of a trace amount of water molecules mixed with acetone is demonstrated here. Briefly, a rectangular strip (dimensions $0.6 \times 2 \times 0.023$ mm^3) of r-GO/agar was fixed onto a rod and dipped inside a glass beaker containing 2.5 mL of liquid acetone. Once completely submerged into the liquid solvent, the strip bends itself into a coiled shape. When a trace amount of liquid water was added to the acetone medium, the coil-shaped strip started opening up. As more water molecules were added in a dropwise manner, the coil-shaped strip started opening up to a greater extent. The entire process was recorded from the top using a digital camera as shown in ESI† Video V3. As can be observed from the snapshots in Fig. 5, the strip could detect the presence of as little as 43.5 μL of water molecules in 2.5 mL of acetone (1.74% of water in acetone), and responded by starting the opening-up process. After the addition of additional liquid water (696 μL), the strip completely opened-up and regained its original position. The mechanism of the real-time sensing of water molecules in the acetone medium is attributed to the different affinities of the r-GO side and agar side of the

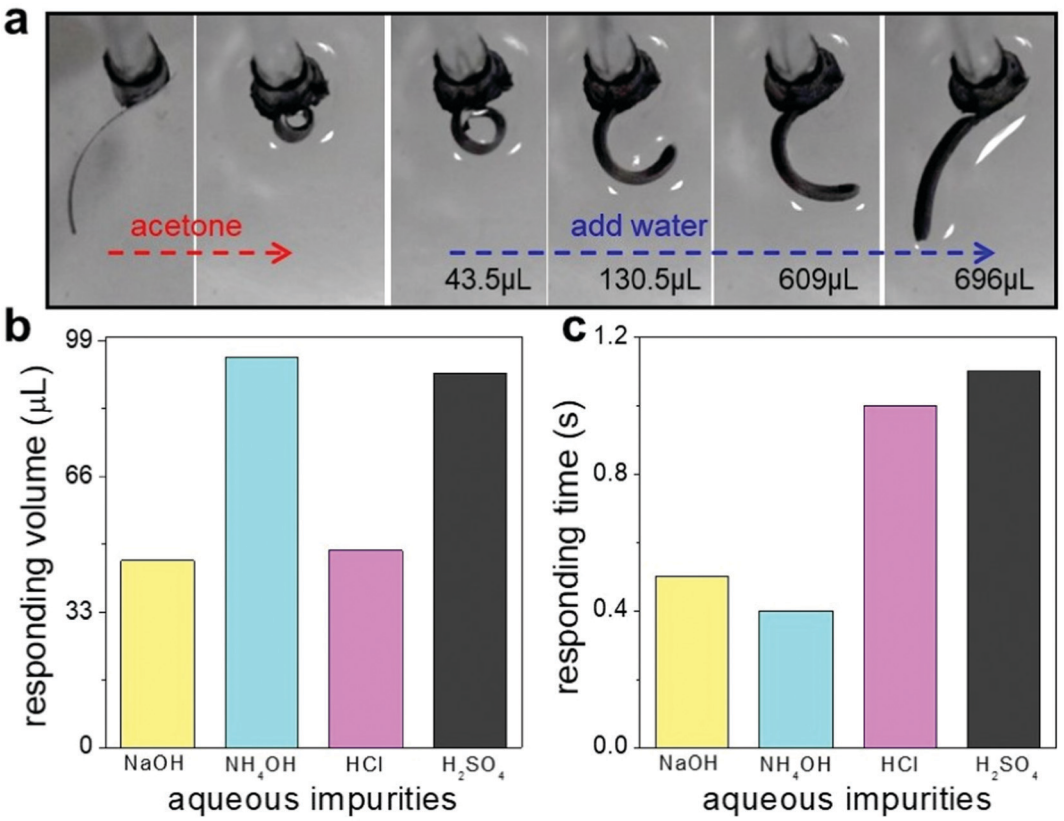

Fig. 5 Detection of liquid contaminants inside a solvent system: (a) snapshots showing the detection of trace amounts of water in acetone by the r-GO/agar bilayer strip. Bar diagrams showing the (b) minimum responding volume and (c) minimum responding time of the r-GO/agar bilayer strip with respect to trace amounts of aqueous impurities mixed in acetone.

bilayer membrane towards water molecules present inside the acetone medium. The interlayer spacing of the r-GO side of the bilayer membrane was found to expand in the acetone medium, whereas it was found to shrink in the presence of water. No such changes were observed in the agar side of the bilayer membrane. These unequal changes prompt asymmetric bending strain along the membrane, which results in changes in the shape of the strips. This observation opened-up a new platform to detect the presence of water molecules inside different solvent systems in a very cost- and time-effective manner. The response time of the r-GO/agar strip in the presence of 43.5 μL of water in acetone was found to be just 1.5 seconds (120° of bending movement). The response time was also found to vary with the varying amount of water molecules present in the acetone medium and hence could provide alternative ways to quantify aqueous contaminants present in the organic medium. Upon addition of 218 μL and 435 μL of water, the response time was found to decrease from 1.5 seconds to 1.25 and 1 second, respectively. The responsiveness of the r-GO/agar strip can also be exploited to detect the nature of the aqueous impurities present in the organic medium. As a proof of concept, the response times and minimum responding volumes of the r-GO/agar strip in the acetone medium were calculated with four aqueous solutions (H_2SO_4, HCl, NaOH and NH_4OH, 1 M each). Even though, upon the addition of all four electrolyte solutions, the strip responded by bending in the same direction, the minimum responding volumes and response times were found to be different in each case (bar diagram in Fig. 5b and c), which could provide valuable information about the type of impurities present in the organic medium. For example, in the cases of HCl and NaOH (concentration of 1 M each), the minimum responding volumes were found to be 48 μL and 45.5 μL, respectively, whereas the response times were found to be 1 s (24° of bending movement) and 0.5 s (18° of bending movement), for HCl and NaOH, respectively. Similarly, in the case of H_2SO_4 and NH_4OH, the minimum responding volumes were found to be 91 μL and 95 μL, respectively. With the minimum responding volumes of H_2SO_4 and NH_4OH, the response times were calculated to be 1.1 s (165° of bending movement) and 0.4 s (161° of bending movement), respectively. The difference in the response time and minimum response volume with different electrolyte solutions is attributed to different miscibility of the electrolytes in acetone.

Apart from the above-mentioned solvent system, the r-GO/agar strip can also detect foreign molecules in a non-aqueous medium. As a proof of concept, the response times and minimum responding volumes of the r-GO/agar strip submersed in toluene solvent were calculated for three different alcohols, namely methanol, ethanol and 2-propanol (Fig. S17, ESI†). All three alcohols responded by bending the strip in a similar direction but displayed different minimum responding volumes and response times. 2-Propanol displayed a minimum responding volume of 73 μL followed by ethanol and methanol with the minimum responding volumes of 96 μL and 110 μL, respectively. With the minimum responding volumes, the response times were calculated to be 1 s (12° of bending movement), 1.5 (7° of bending movement) and 1.75 s (8° of bending movement) for 2-propanol, ethanol and methanol, respectively. The difference in miscibility of the three alcohols with toluene is attributed for the difference in minimum responding volumes and responding times.

Conclusion

In conclusion, we have demonstrated the possibility of applying reconstructed layered material-based responsive membranes for detecting contaminants dissolved in liquid media. The shape of the bilayer strip prepared by re-stacking exfoliated layered materials is determined by the balance between the mechanical properties of the individual components. When soaked-in, liquid molecules interact with the two-dimensional building blocks of the lamellar membranes and influence the attractive and repulsive forces between the layers and hence alter their mechanical properties. As a result, the shape of the materials becomes dependent on the surrounding atmosphere. The presence of foreign molecules/impurities interferes with the interactions between the liquid molecules and nano-building blocks as well as the attractive/repulsive forces among the 2D nanomaterials, and hence it influences their shape-morphing properties. Here, the bilayer membrane of r-GO/agar taken as an example exhibits remarkable under-liquid robustness. Numerous times of soaking/bending into solvents of diverse chemical nature did not seem to alter its mechanical robustness and shape-morphing properties. Responsive materials with this robustness and specific bending and recovering speed with different solvent molecules could provide a new kind of platform to develop electronics-free inexpensive sensors of solvent molecules and solvent composition. Moreover, the fabrication process of this kind of bilayer membrane can be easily scaled up to prepare large area free-standing smart membranes in a very cost-effective manner. It is worth mentioning that the bending performance of the bilayer-based actuator is dependent on multiple parameters, such as the size of the vessel, the distance of the actuator to the surface of the vessel, the shape and thickness of the actuators and so on. However, inconsistencies arising from these parameters can be minimized through appropriate control experiments and optimization of the device structure.

Conflicts of interest

The authors declare no competing financial interest.

Acknowledgements

K. R. acknowledges the Core Research Grant (CRG/2020/002943) of the Science and Engineering Research Board (SERB), India. All the authors acknowledge the Central Instruments Facility (CIF), IIT Guwahati, for their help with sample characterization. A. B. N., R. K. G., P. D., T. J. K. and B. R. B. are grateful to IITG for PhD fellowships.

References

1 B. Jakoby and M. J. Vellekoop, Physical sensors for water-in-oil emulsions, *Sens. Actuators, A*, 2004, **110**, 28–32.
2 N. S. Foster, J. E. Amonette, T. Autrey and J. T. Ho, Detection of trace levels of water in oil by photoacoustic spectroscopy, *Sens. Actuators, B*, 2001, **77**, 620–624.
3 Y. Ooyama, M. Sumomogi, T. Nagano, K. Kushimoto, K. Komaguchi, I. Imae and Y. Harima, Detection of water in organic solvents by photo-induced electron transfer method, *Org. Biomol. Chem.*, 2011, **9**, 1314–1316.
4 W. Chen, Z. Zhang, X. Li, H. Ågren and J. Su, Highly sensitive detection of low-level water content in organic solvents and cyanide in aqueous media using novel solvatochromic AIEE fluorophores, *RSC Adv.*, 2015, **5**, 12191–12201.
5 J.-G. Yu, X.-H. Zhao, H. Yang, X.-H. Chen, Q. Yang, L.-Y. Yu, J.-H. Jiang and X.-Q. Chen, Aqueous adsorption and removal of organic contaminants by carbon nanotubes, *Sci. Total Environ.*, 2014, **482**, 241–251.
6 V. Pichon, Solid-phase extraction for multiresidue analysis of organic contaminants in water, *J. Chromatogr. A*, 2000, **885**, 195–215.
7 D. Kou, S. Zhang, J. L. Lutkenhaus, L. Wang, B. Tang and W. Ma, Porous organic/inorganic hybrid one-dimensional photonic crystals for rapid visual detection of organic solvents, *J. Mater. Chem. C*, 2018, **6**, 2704–2711.
8 Z. Wang, J. Zhang, J. Li, J. Xie, Y. Li, S. Liang, Z. Tian, C. Li, Z. Wang, T. Wang, H. Zhang and B. Yang, Colorful detection of organic solvents based on responsive organic/inorganic hybrid one-dimensional photonic crystals, *J. Mater. Chem.*, 2011, **21**, 1264–1270.
9 M. Qing, H. Liang, J. Zhang and H. Zhan, The mechanism of detecting water content in oil–water emulsions using impedance spectroscopy, *J. Pet. Sci. Eng.*, 2020, **188**, 106863.
10 K. Allsopp, I. Wright, D. Lastockin, K. Mirotchnik and A. Kantzas, Determination of Oil and Water Compositions of Oil/Water Emulsions Using Low Field NMR Relaxometry, *J. Can. Pet. Technol.*, 2001, **40**, 58–61.
11 C. Ye, Y. Qin, P. Huang, A. Chen and F.-Y. Wu, Facile synthesis of carbon nanodots with surface state-modulated fluorescence for highly sensitive and real-time detection of water in organic solvents, *Anal. Chim. Acta*, 2018, **1034**, 144–152.
12 Y. Zhou, D. Zhang, W. Xing, J. Cuan, Y. Hu, Y. Cao and N. Gan, Ratiometric and Turn-On Luminescence Detection of Water in Organic Solvents Using a Responsive Europium-Organic Framework, *Anal. Chem.*, 2019, **91**, 4845–4851.
13 T.-I. Kim and Y. Kim, A Water Indicator Strip: instantaneous Fluorogenic Detection of Water in Organic Solvents, Drugs, and Foodstuffs, *Anal. Chem.*, 2017, **89**, 3768–3772.
14 F. Cheng, R. Fu, Y. Wen, Y.-Y. Yang, C. Zeng, Y. Zhang, S. Hu and X. Wu, A new Cd based metal-organic framework for quick and convenient detection of trace water in isopropanol and 1,4-dioxane, *J. Mater. Chem. C*, 2018, **6**, 12341–12346.
15 J. Zhang, J. Wu, G. Tang, J. Feng, F. Luo, B. Xu and C. Zhang, Multiresponsive water-stable luminescent Cd coordination polymer for detection of TNP and Cu^{2+}, *Sens. Actuators, B*, 2018, **272**, 166–174.
16 Z. Chen, D. Zhang, E. Peng and J. Ding, 3D-printed ceramic structures with in situ grown whiskers for effective oil/water separation, *Chem. Eng. J.*, 2019, **373**, 1223–1232.
17 H. Sun, B. Wang and S. G. DiMagno, A Method for Detecting Water in Organic Solvents, *Org. Lett.*, 2008, **10**, 4413–4416.
18 T. Wang and H. Li, A Red-Emitting Luminescent Material Capable of Detecting Low Water Content in Organic Solvents, *Chem. – Eur. J.*, 2016, **22**, 12400–12405.
19 R. K. Gogoi, A. B. Neog, N. Sarmah and K. Raidongia, Preparation of responsive bilayer membrane through morphological tuning of nano-scale building blocks, *J. Mater. Chem. A*, 2019, **7**, 21157–21167.
20 H.-J. Kim, S.-H. Song and S.-H. Ahn, A turtle-like swimming robot using a smart soft composite (SSC) structure, *Smart Mater. Struct.*, 2012, **22**, 014007.
21 M. Sponchioni, U. Capasso Palmiero and D. Moscatelli, Thermo-responsive polymers: applications of smart materials in drug delivery and tissue engineering, *Mater. Sci. Eng., C*, 2019, **102**, 589–605.
22 S. Y. Yang, K. H. Cho, Y. Kim, M.-G. Song, H. S. Jung, J. W. Yoo, H. Moon, J. C. Koo, J.-D. Nam and H. R. Choi, High performance twisted and coiled soft actuator with spandex fiber for artificial muscles, *Smart Mater. Struct.*, 2017, **26**, 105025.
23 A. Basheer Al, Advances in the smart materials applications in the aerospace industries, *Aircr. Eng.*, 2020, **92**, 1027–1035.
24 P. J. Roth and A. B. Lowe, Stimulus-responsive polymers, *Polym. Chem.*, 2017, **8**, 10–11.
25 J. W. Sohn, G.-W. Kim and S.-B. Choi, A state-of-the-art review on robots and medical devices using smart fluids and shape memory alloys, *Appl. Sci.*, 2018, **8**, 1928.
26 A. Lai, Z. Du, C. L. Gan and C. A. Schuh, Shape Memory and Superelastic Ceramics at Small Scales, *Science*, 2013, **341**, 1505–1508.
27 X. Yu, H. Cheng, M. Zhang, Y. Zhao, L. Qu and G. Shi, Graphene-based smart materials, *Nat. Rev. Mater.*, 2017, **2**, 17046.
28 R. K. Gogoi and K. Raidongia, Strategic Shuffling of Clay Layers to Imbue Them with Responsiveness, *Adv. Mater.*, 2017, **29**, 1701164.
29 R. K. Gogoi, K. Saha, J. Deka, D. Brahma and K. Raidongia, Solvent-driven responsive bilayer membranes of clay and graphene oxide, *J. Mater. Chem. A*, 2017, **5**, 3523–3533.
30 R. K. Gogoi and K. Raidongia, Intercalating cation specific self-repairing of vermiculite nanofluidic membrane, *J. Mater. Chem. A*, 2018, **6**, 21990–21998.
31 C. Wang, Y. Wang, Y. Yao, W. Luo, J. Wan, J. Dai, E. Hitz, K. Fu and L. Hu, A Solution-Processed High-Temperature, Flexible, Thin-Film Actuator, *Adv. Mater.*, 2016, **28**, 8618–8624.
32 D.-D. Han, Y.-L. Zhang, Y. Liu, Y.-Q. Liu, H.-B. Jiang, B. Han, X.-Y. Fu, H. Ding, H.-L. Xu and H.-B. Sun, Bioinspired Graphene Actuators Prepared by Unilateral UV Irradiation of Graphene Oxide Papers, *Adv. Funct. Mater.*, 2015, **25**, 4548–4557.

33 H. Bi, K. Yin, X. Xie, Y. Zhou, S. Wan, F. Banhart and L. Sun, Microscopic bimetallic actuator based on a bilayer of graphene and graphene oxide, *Nanoscale*, 2013, **5**, 9123–9128.
34 S. Park, J. An, J. W. Suk and R. S. Ruoff, Graphene-Based Actuators, *Small*, 2010, **6**, 210–212.
35 J. Xue, Z. Gao and L. Xiao, The Application of Stimuli-Sensitive Actuators Based on Graphene Materials, *Front. Chem.*, 2019, **7**, 803.
36 X. Xie, L. Qu, C. Zhou, Y. Li, J. Zhu, H. Bai, G. Shi and L. Dai, An Asymmetrically Surface-Modified Graphene Film Electrochemical Actuator, *ACS Nano*, 2010, **4**, 6050–6054.
37 J. Liu, Z. Wang, X. Xie, H. Cheng, Y. Zhao and L. Qu, A rationally-designed synergetic polypyrrole/graphene bilayer actuator, *J. Mater. Chem.*, 2012, **22**, 4015–4020.
38 E. Palleau, D. Morales, M. D. Dickey and O. D. Velev, Reversible patterning and actuation of hydrogels by electrically assisted ionoprinting, *Nat. Commun.*, 2013, **4**, 2257.
39 Q. Zhao, J. Heyda, J. Dzubiella, K. Täuber, J. W. C. Dunlop and J. Yuan, Sensing solvents with ultra-sensitive porous poly(ionic liquid) actuators, *Adv. Mater.*, 2015, **27**, 2913–2917.
40 Y. Haldorai and J.-J. Shim, Chemo-responsive bilayer actuator film: fabrication, characterization and actuator response, *New J. Chem.*, 2014, **38**, 2653–2659.
41 A. Toncheva, B. Willocq, F. Khelifa, O. Douheret, P. Lambert, P. Dubois and J.-M. Raquez, Bilayer solvent and vapour-triggered actuators made of cross-linked polymer architectures *via* Diels–Alder pathways, *J. Mater. Chem. B*, 2017, **5**, 5556–5563.
42 A. B. Neog, R. K. Gogoi, T. Dutta and K. Raidongia, Electrical Actuation of Hydrophobic Bilayer Membranes of Reduced Graphene Oxide and Agar for Inducing Chemical Reactions in Microdroplets, *ACS Appl. Nano Mater.*, 2020, **3**, 6629–6635.
43 R. Zeng, Z. Luo, L. Zhang and D. Tang, Platinum Nanozyme-Catalyzed Gas Generation for Pressure-Based Bioassay Using Polyaniline Nanowires-Functionalized Graphene Oxide Framework, *Anal. Chem.*, 2018, **90**, 12299–12306.
44 J. Shu, Z. Qiu and D. Tang, Self-Referenced Smartphone Imaging for Visual Screening of H_2S Using Cu_xO–Polypyrrole Conductive Aerogel Doped with Graphene Oxide Framework, *Anal. Chem.*, 2018, **90**, 9691–9694.
45 G. Cai, Z. Yu, R. Ren and D. Tang, Exciton–Plasmon Interaction between AuNPs/Graphene Nanohybrids and CdS Quantum Dots/TiO_2 for Photoelectrochemical Aptasensing of Prostate-Specific Antigen, *ACS Sens.*, 2018, **3**, 632–639.
46 Q. Zhou, Y. Lin, K. Zhang, M. Li and D. Tang, Reduced graphene oxide/$BiFeO_3$ nanohybrids-based signal-on photoelectrochemical sensing system for prostate-specific antigen detection coupling with magnetic microfluidic device, *Biosens. Bioelectron.*, 2018, **101**, 146–152.
47 Q. Zhou, Y. Lin, J. Shu, K. Zhang, Z. Yu and D. Tang, Reduced graphene oxide-functionalized FeOOH for signal-on photoelectrochemical sensing of prostate-specific antigen with bioresponsive controlled release system, *Biosens. Bioelectron.*, 2017, **98**, 15–21.